A COMPUTATIONAL STUDY OF FLAME DYNAMICS ON SOOT PRODUCTION AND TRANSPORT FOR AN ACETYLENE-AIR LAMINAR DIFFUSION FLAME IN THE FIELD OF A CONVECTING LINE VORTEX

S. Mishra and S. Basu
Email: sbasu@mecheng.iisc.ernet.in (S.Basu)
Department of Mechanical Engineering, Indian Institute of Science, Bangalore 560012

ABSTRACT

The present work involves a computational study of soot formation and transport in case of a laminar acetylene diffusion flame perturbed by a convecting line vortex. The topology of the soot contours (as in an earlier experimental work [4]) have been investigated. More soot was produced when vortex was introduced from the air side in comparison to a fuel side vortex. Also the soot topography was more diffused in case of the air side vortex. The computational model was found to be in good agreement with the experimental work [4]. The computational simulation enabled a study of the various parameters affecting soot transport. Temperatures were found to be higher in case of air side vortex as compared to a fuel side vortex. In case of the fuel side vortex, abundance of fuel in the vortex core resulted in stoichiometrically rich combustion in the vortex core, and more discrete soot topography. Overall soot production too was low. In case of the air side vortex abundance of air in the core resulted in higher temperatures and more soot yield.
Statistical techniques like probability density function, correlation coefficient and conditional probability function were introduced to explain the transient dependence of soot yield and transport on various parameters like temperature, acetylene concentration.

INTRODUCTION

There have been numerous computational studies on the simulation of laminar unsteady diffusion flames over the past two decades. A good understanding of the dynamics of laminar flames is helpful in dealing with the complexities of turbulent flames. Thus increased attention has focused on studies using transient models to adequately characterize the fluctuating behaviour of these flames. Since many practical combustion devices involve sooting hydrocarbon diffusion flames, like gas turbines combustors, some of the recent efforts have also focused on studies which include the processes of soot formation and its transport. [1][2][3] The purpose of the present paper is to study the effects of spatial and temporal evolution of an unsteady acetylene/air laminar diffusion flame perturbed by a line vortex and the corresponding effects on soot production and transport. Soot topology formed on the interaction of a two-dimensional line vortex with a laminar 2D diffusion flame were analysed and studied computationally. Previously, in literature the authors have published an experimental study of the same. In the experimental study, a planar diffusion flame was established between two parallely flowing, equal velocity streams of acetylene (diluted with nitrogen) and air. Line vortices from air or fuel side were generated on demand in the flow apparatus [4]. As reported in the paper, the soot topography and amount of soot produced

differed significantly when the line vortex was introduced from air side in comparison to the line vortex of same intensity introduced from the fuel side. Similar conditions and design (as in [4]) were used in our computational model. A five species single step combustion model of acetylene with air was employed. The soot formation model was a four-step, two-equation, two- moment model adapted from Leung et al [5]. The analysis conducted using the computational model has the objectives of trying to examine and understand the physics of soot formation and transport during flame vortex interaction. This simulation in essence focuses on (a) gaining more insight into how the induction of a line vortex near a flame affects the soot production and distribution hence forth, and (b) explaining the reasons for the difference in the contours and intensity of soot formed when vortex is induced from the air side and from the fuel side. In our study, heat, mass and momentum transport processes in the field of a line vortex have been found to bear fundamental effects on both soot formation and distribution. The location and extent of reaction zones lead to asymmetry between the two cases of vortex induction from the fuel side and air side. It is proposed that the analysis of the results of the computational model at different Vortex Reynolds numbers will throw light on the transport phenomenon taking place in such cases, which can provide important inputs for design purposes in combustion engineering [6][7].

SOOT MODEL

In this study Lindstedt [5] model was used for soot nucleation, growth and coagulation, and Lee's model for oxidation [8]. The two-equation, four-step, two-moment soot formation model has been used extensively in past studies on laminar and turbulent diffusion flames [9]. The model can be explained as follows. First soot nucleates to form the smallest stable soot particles. Diameter of the nascent soot particles is taken to be about 1nm, constituting of about 100 carbon atoms [5]. Soot particles then exhibit growth both by surface growth of individual particles and coagulation of two or more particles. Coagulation of soot particles results in a decrease in the soot particle density. Surface growth of individual particles leads to an increase in the soot mass fraction and the oxidation step leads to a decrease in the soot mass fraction [5]. On solving the governing equations of species mass fraction, mass, momentum and energy along with the equations of soot formation and transport, patterns of species mass concentration, temperature, velocity/vorticity distribution, soot contours and rates of different steps of soot production etc. are obtained, which provide qualitative and quantitative insights. The density of soot formed is taken as 2000.0 kg/m^3 [9][10][11] . The nucleation step (the first step) is given by: [5]

$$C_2H_2 \rightarrow 2C(s) + H_2$$

$$R_1 = k_1(T)\,[C_2H_2]\ [\text{kmol/m}^3/\text{s}] \quad (1)$$

$$k_1(T) = 0.1*10^5\, e^{-21,000/T}\ [1/\text{s}] \quad (2)$$

The surface growth step (the second step) is given by: [5]

$$C_2H_2 + nC(s) \rightarrow (n+2)\,C(s) + H_2$$

$$R_2 = k_2(T)\,f(S)\,[C_2H_2] \quad [\text{kmol/m}^3/\text{s}] \quad (3)$$

$$k_2(T) = 0.6*10^4 e^{-12,000/T} \quad [\text{m}^{3/2}/\text{m-soot/s}] \quad (4)$$

$$S = \pi\,(d_p^2)(\rho N_s) \quad (5)$$

$$d_p = (6/\pi)(1/\rho_{C(s)})(Y_s/N_s)\ ; \quad (6)$$

$$f(S) = \sqrt{(S)} \quad (7)$$

The agglomeration step is given by: [5]

$$nC(s) \rightarrow C_n(s)$$

$$R_3 = -2*C_a d_p^{1/2}(6\kappa T/\rho_{C(s)})*(\rho N_s)^2 \quad [kmol/m^3/s] \quad (8)$$

$$C_a = 9.0$$

The oxidation step is given by: [8]

$$C(s) + 1/2O_2 \rightarrow CO$$

$$R_4 = k_4(T)\, S\, [O_2] \quad [kmol/m^3/s] \quad (9)$$

$$k_4(T) = 0.1*10^5 e^{-19,680/T} \quad [m^{3/2}/m\text{-soot/s}] \quad (10)$$

$$S = \pi (d_p^2)(\rho N_s) \quad (11)$$

The thermophoretic velocity of soot used in our study is based on the work of Waldmann [12][13]. It is given by

$$V_{th} = -\frac{3\nu}{4\left(1 + \frac{\pi}{8}\alpha_m\right)}\frac{\nabla T}{T} \quad (12)$$

α_m is the accommodating factor and is generally taken as 1.0. [14][15].
It was incorporated in the user defined functions of soot particle and mass sources so that the particle number density and soot mass fraction remain conserved scalars. A more detailed description of the soot model can be found in ref. 5.

COMPUTATIONAL MODEL

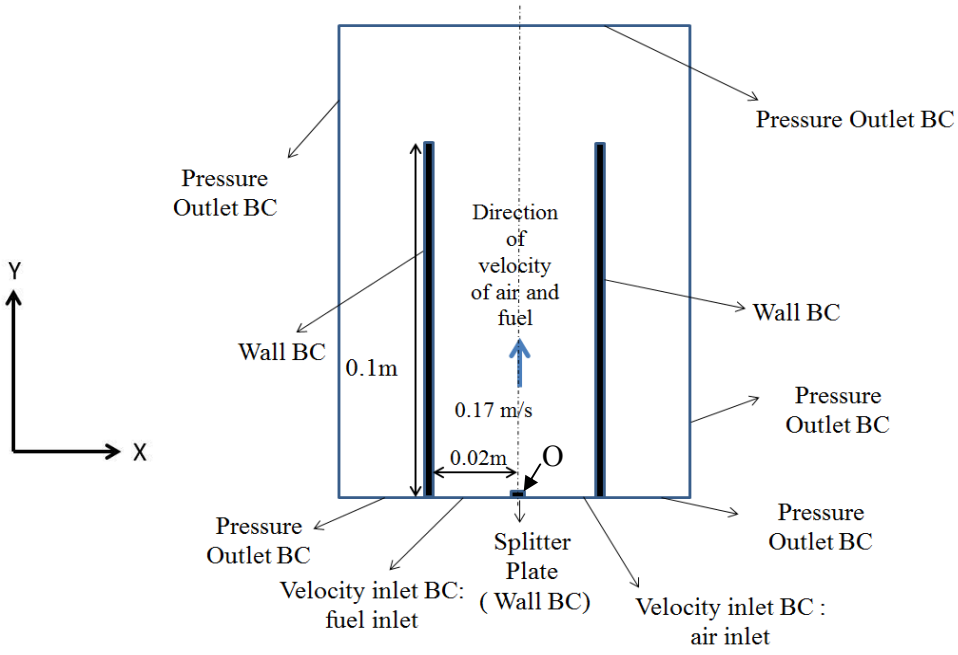

Figure 1. The computational domain and the boundary conditions (O is the origin)

The computational model employed (fluent 6.3.26) solves the two-dimensional, incompressible, and time-dependent, reactive-flow Navier-Stokes equations coupled with the aforementioned sub-models for soot formation. Qualitative comparisons between the experimental and computed flame temperatures and soot particle density show good agreement with the existing literature on soot production in acetylene laminar flames [16][17][18].Further on introduction of line vortex from air and fuel sides, the soot intensity and soot mass fractions predicted by our model are in confirmation to the observations in ref. 4.A second order implicit method and a pressure based solver is used. Both the soot mass per unit volume and soot particle number density are incorporated as user defined scalars. The soot volume fraction, particle number density and temperature of flame were found to be in good agreement with similar works reported in the literature [16][17][18]. Fig.1 shows the computational domain of the study figure with the different boundary conditions. The incoming streams of fuel and air form a laminar diffusion layer. Time steps were non-dimensionalised by the time taken by the streams to cover the full 0.1 m length at a convective velocity of 0.17 m/s i.e. about 0.5882 seconds. t* is the non-dimensional time. Vortex was introduced from fuel side or air side on demand by applying a time dependent velocity boundary condition on the side from which vortex needs to be initiated. The velocity impulse given was same as that given in [4] and was given at t* = 2.754. The spatial domain of data collection for statistical analyses at the non-dimensional time step of 3.06 extends from -0.2m to +0.2m in X direction and from 0.0 m to 0.7 m in Y direction. The domain is moved at the convective velocity of fuel and air stream i.e. at 0.17 m/s at the non-dimensional time of 3.4.

RESULTS AND DISCUSSION

In this section, first an analysis based on temperature contours and physical reasoning is conducted which is followed by a comparison of computational results with the experimental results in [4]. After putting in place the basic premises and reasoning, we move on to a statistical analysis using probability density functions (pdfs) followed by an analysis using Pearson's correlation coefficient.

TIME MARCHING – CONTOURS OF TEMPERATURE AND THE FLAME FRONT

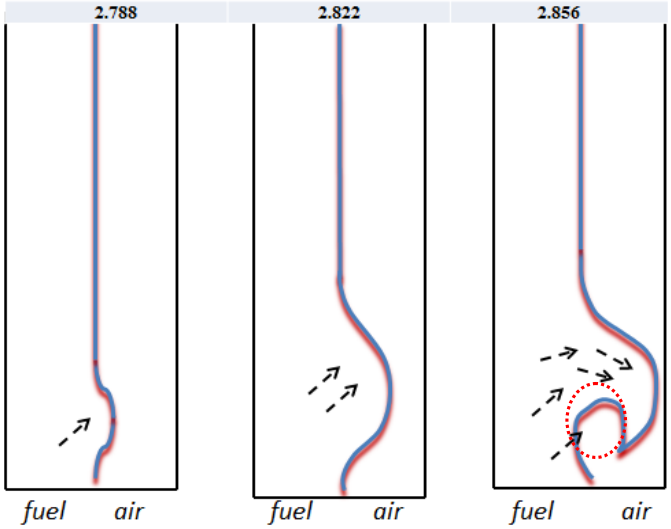

Figure 2. Schematic showing dynamics of fuel side vortex

The vortex is introduced from the fuel side at the non-dimensional time (t*) of 2.754, Figure 2 shows the shape of flame at three ensuing time steps, spaced at equal intervals of t*. The dashed arrows show the direction of fuel flow at these instances. The fuel stream comprises of acetylene and nitrogen with acetylene mole fraction of 0.25. Thus, the mass flow rate of acetylene in the fuel stream, is three times higher than what is required for complete combustion based on the mass flow rate of the air stream. Fuel stream, due to the high momentum imparted for vortex generation tries to shift the flame front more towards the oxidizer side and starts to fill the core of the developing vortex, which has been shown by a dotted red color circle. Since more fuel is present than required in the incoming fuel stream, the flame shifts more towards the outer periphery of the vortex that is being developed. This translates to lower amount of oxidizer present in the vortex core and hence the fuel present in the core is not able to undergo complete combustion. Lower temperatures are hence observed in the core. Acetylene, present is the vortex core is transported out from the core due to centrifugal force and diffusion, till it reacts with oxygen present at the periphery, thus feeding the flame from the inside of the vortex. The temperature is consistently higher on the outer periphery of the vortex as compared to the inner regions. Less soot is thus produced in the vortex core than at the periphery. The overall temperature is lower as compared to when the vortex is introduced from the air side resulting in lower overall amount of soot. This is because soot production rates are exponentially dependent on temperature whereas linearly dependent on chemical species concentrations. In the case of the fuel side vortex, the soot contours remain more discrete, as the vortex tries to wrap the air stream and combustion is not able to take place homogeneously throughout the vortex, due to the locally lean stoichiometry topology. This results in lower spatial temperature gradients. Thermophoretic transport, which dominates over diffusive transport in case of soot, is not strong enough to allow spatial homogenization of soot. This aspect is also discussed in the correlations section. When the vortex is introduced from the air side at the non-dimensional time t* of 2.754, Figure 3 shows the shape of flame at three ensuing time steps, spaced at equal intervals of time.

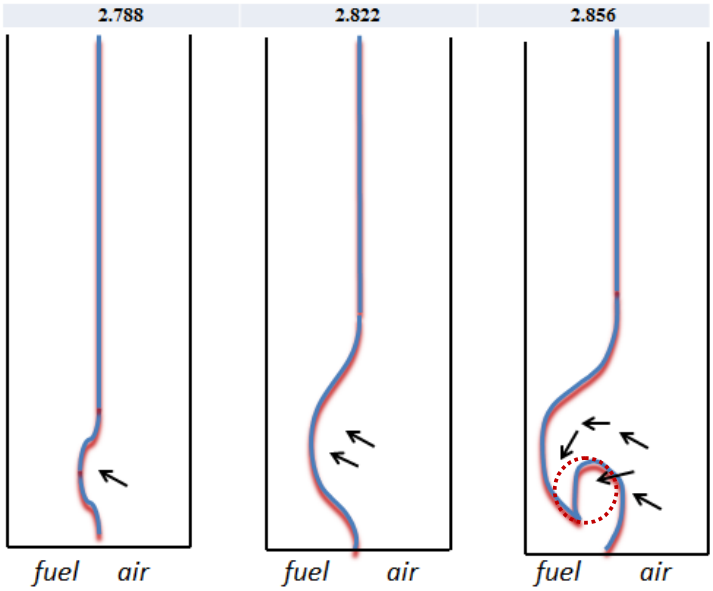

Figure 3. Schematic showing effects of air side vortex

The solid arrows show the direction of air flow at these instances. Air stream, due to the relatively higher momentum tries to shift the flame front more towards the fuel side and starts to occupy the core of the developing vortex, which has been shown by a dotted red color

circle. This results in higher amounts of oxidizer present in the vortex core compared to local concentration of fuel. Hence higher temperatures are observed in the core due to more complete nature of the combustion taking place. The temperatures are higher in the inner regions of the vortex as compared to the periphery. More soot is thus produced in the vortex core than at the periphery. The overall temperature is higher as compared to when the vortex is introduced from the fuel side resulting in higher overall amount of soot due to exponential dependence of soot formation rates on temperature whereas a linear dependence on the concentration of chemical species. Soot, present in the vortex core diffuses out from the core due to centrifugal force, thermophoretic transport, advection and diffusion. A more diffuse contour of soot is observed in case of vortex from the air side. The higher temperature gradients resulting from complete combustion lead to higher transport of soot due to centrifugal forces and thermophoretic effect resulting in a more homogenous distribution of soot. Figs. 4a-b show the temperature profile or the flame shape on the introduction of vortex from the fuel and air side at three time steps at equal intervals of time. Black arrows indicate the direction of movement of fuel whereas white arrows indicate the direction of movement of oxidizer. When the vortex is introduced from the fuel side, as shown in the figure, the flame front is not able to reach the core which contains abundance of fuel. The momentum from vortex induction keeps the flame front away from the vortex core and on the periphery. As the core develops further it gets richer with acetylene and leaner in oxidizer leading to lower temperatures and hence lesser soot yield. The churning and wraping effects of vortex, centrifugal forces, thermophoretic diffusion and advection transport make the distribution of soot more diffuse in and around the core.

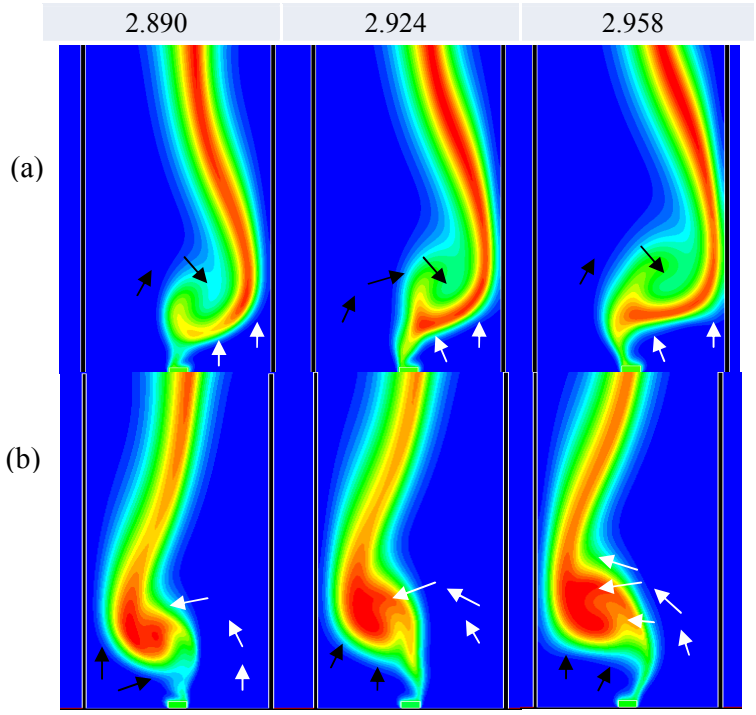

Figure 4. Contours maps of temperature at different time steps (on the top of the figure in non-dimensionalised form) (a) fuel side vortex (b) air side vortex

TOPOLOGIES OF T, N_S AND W

As observed in our model, the presence of a vortex changes the temperature distribution and its spatial gradient in a manner which results in transport of chemical species, leading way to

changes in the spatial and temporal distribution of the chemical species and chemical reactions. This results in differences in the production and distribution of soot in and around the core of the vortex. Thermophoretic velocity of soot, which is a function of temperature gradient and plays a major role in its transport, is found to have a significant effect in the resulting topography [3][19]. Thus we have spatial and temporal differences in soot intensities and contours both when vortex is induced from air side and from the fuel side. The soot formation contours as shown in Figs 5 & 6 formed after the introduction of line vortex from fuel and air sides were compared with the previous experimental study (Fig 5a & 5b and Figs 6a & 6b [4]). As can be seen the comparison between the experimental and computational results are very reasonable.

Figures 5c, 5d and 5e show the soot particle density (N_S), Temperature (T) and vorticity contours when vortex is induced from air side in the model (Figure 5b). Figures 6c, 6d and 6e show the same contours for fuel side vortex. Experimentally observed contours are shown in Figures 5a and 6a [4]. Experimentally the soot is found to be distributed in and around the vortex core in diffuse layers (for air side vortex) and qualitatively resemble the numerical profiles in Figure 5c. The effect of temperature profile on the soot generation is clearly evident in Figures 5c and 6c since lower temperatures in the vortex core lead to lower soot production.

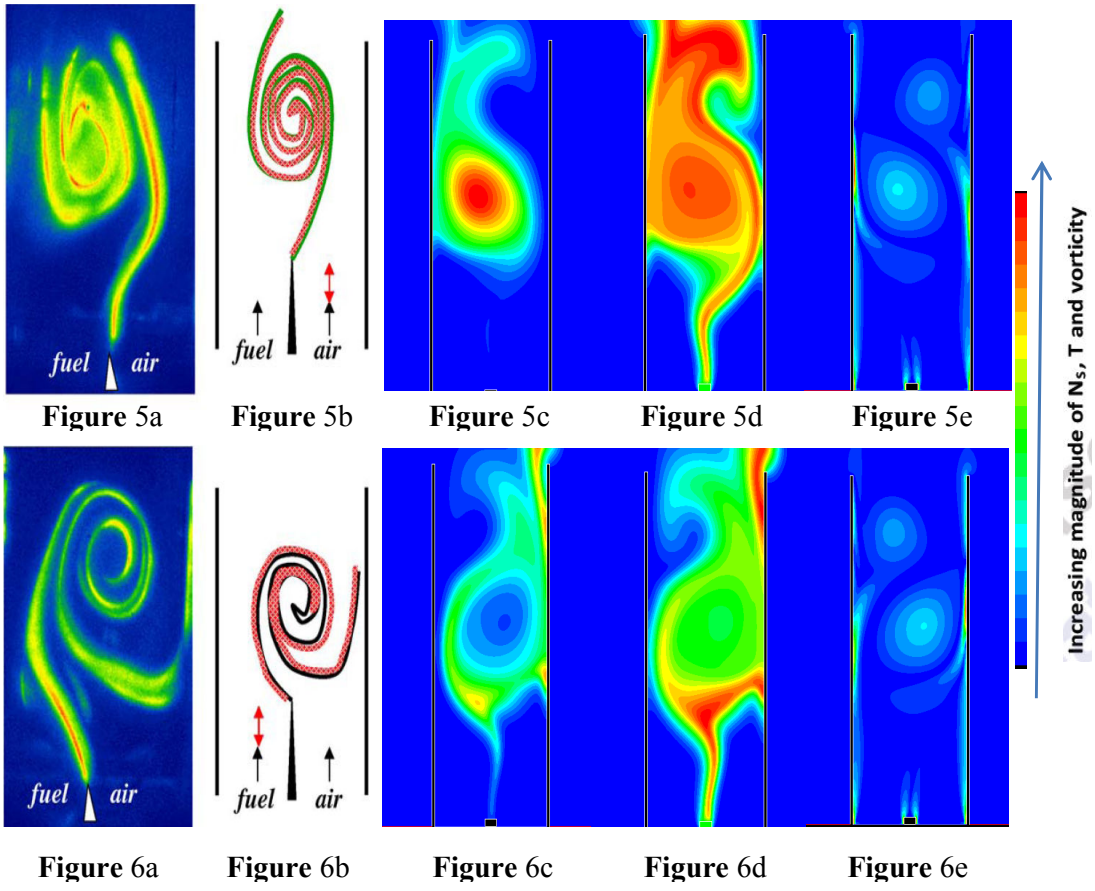

Figure 5a **Figure** 5b **Figure** 5c **Figure** 5d **Figure** 5e

Figure 6a **Figure** 6b **Figure** 6c **Figure** 6d **Figure** 6e

Figure 5: a.) Experimental determined soot mass fraction for air side vortex, b.) Air side vortex, Computationally determined contours of c.) soot particle density, d.) temperature, e.) vorticity for air side vortex

Figure 6: a.) Experimental determined soot mass fraction for fuel side vortex, b.) fuel side vortex, Computationally determined contours of c.) soot particle density, d.) temperature, e.) vorticity for fuel side vortex

In contrast, topography of soot in vortices interacting from the fuel side is such that soot is confined to thinner layers around the vortex core which does not contain any soot [4] as shown in Figure 6a. This also matches with the observations in our computational model as shown in Figure 6c. Effect of the spatial distribution of temperature is again evident in Figure 6d. It is also observed that the vortices interacting with the flame from the air side produce more soot in comparison to vortices interacting from fuel side.

PROBABILITY DENDITY FUNCTIONS (pdfs)

The probability density functions (pdf) of absolute temperature (Fig 7) and the pdfs of normalized soot mass fractions (Y_s/Y_{s_max}), acetylene molar concentrations ($[C_2H_2]/[C_2H_2]_{max}$) , thermophoretic velocity (V_{th}/V_{th_max}) and soot particle diameter (d_p/d_{p_max}) throw light on the soot production and transport . Fig 8 & 9 show the four normalised pdfs both in case of vortex induced from air side and fuel side at two different t* after the introduction of the vortex. The bin size for generating the pdfs has been taken to be equal to 100.

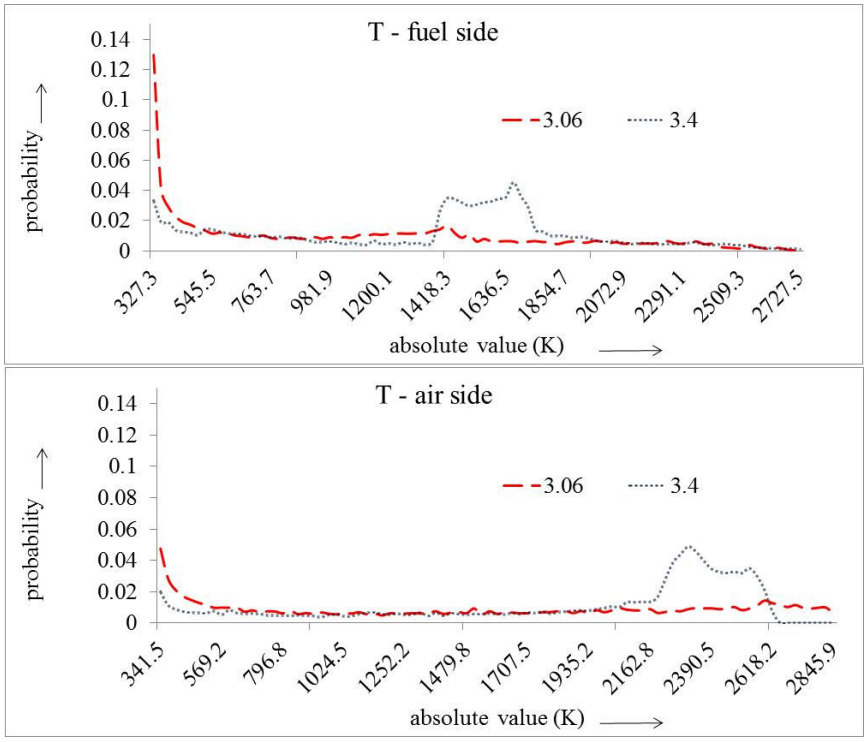

Figure7. PDF of absolute temperature: fuel & air side vortex

The lower temperatures in case of fuel side vortex are reflected in the Fig.7 which shows that the probability of finding lower temperatures is more in this case as compared to vortex from the air side and as expected, temperatures increase in both cases with time.

Absolute temperature is higher in case of air side vortex resulting from more combustion and hence higher soot yield whereas it is reverse in the case of a fuel side vortex. Although comparatively lesser amount of acetylene is available for soot formation in case of air side vortex more soot is formed since soot formation has a linear dependence on acetylene and oxygen concentrations but an exponential dependence on temperature. Mean temperatures are higher by more than 500 K in case of air side vortex as compared to fuel side vortex.

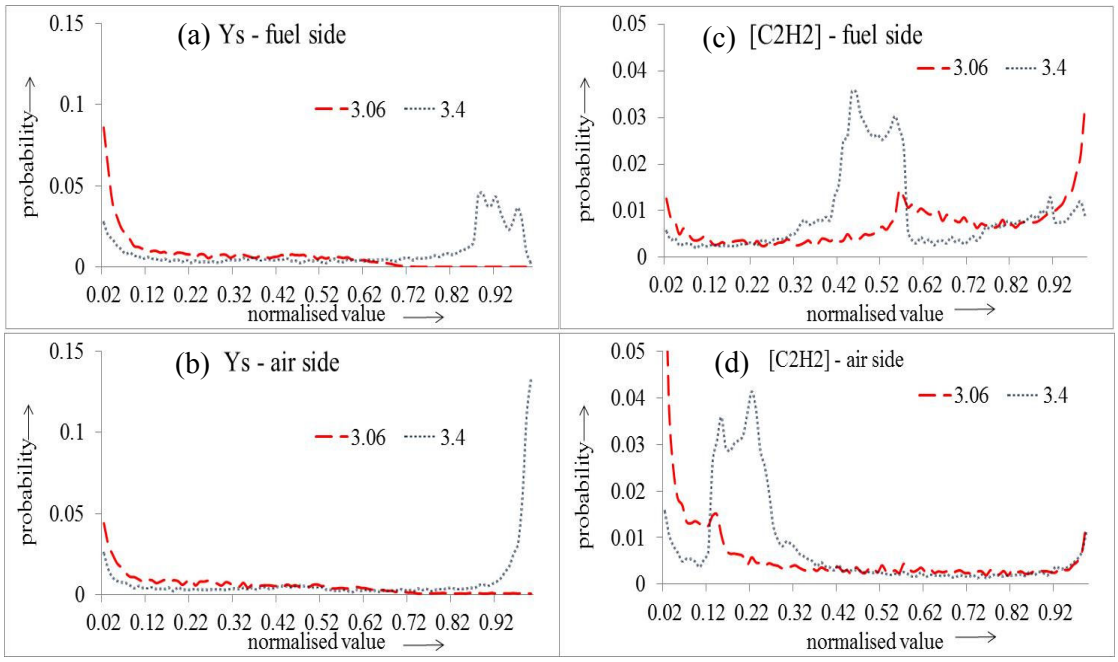

Figure 8. PDFs of soot mass fraction and acetylene concentration: fuel side & air side vortices

The pdf of Y_s in cases of vortex (Fig 8a & 8b) induced from air side shows that more soot is produced since the probability is higher for soot mass fraction closer to Y_{s_max}.The pdfs for Y_s were clipped off at both the ends since probabilities will be higher for the two extremes, namely 0 &1. In the case of fuel side vortex, the corresponding probabilities are lower. Acetylene concentration (Fig 8c & 8d) is lower in case of air side vortex, due to more complete combustion, resulting in higher temperatures and thus producing more soot. This as mentioned earlier is due to the exponential dependence on temperature, whereas in case of fuel side vortex more acetylene is left unreacted leading to lower temperatures and hence lower soot mass fraction.

The distribution of thermophoretic transport is quite similar though and remains so with time, according to the pdfs. The absolute magnitudes of mean temperature gradients in the domain of statistical study are about an order of magnitude higher in case of air side vortex in comparison to the fuel side vortex. The standard deviation in the magnitudes of temperature gradients too is about an order of magnitude higher in case of air side vortex. The effect of thermophoretic transport is also discussed in the next section using the pearson's correlation coefficient as it helps in understanding the different soot contours as observed in [4].

Similar distribution of thermophoretic velocities (Figs 9a & 9b) in the two cases, but higher temperatures and temperature gradients in the former (air side vortex), lead to more soot production and spatially homogeneous distribution in the former case than in the latter case, in and around the vortex core. Soot production is higher in the former case leading to more soot in the core as compared to the latter case where less soot is observed in the soot core. The thermophoretic transport though distributed similarly, is higher in case of air side vortex, as the mean thermophoretic velocity is about double in case of air side vortex as compared to the fuel side vortex in the domain of statistical study. Centrifugal forces and thermophoretic force to lead to a more diffuse soot topography in case of air side vortex, which is supported by the experimental evidence by Cetegen and Basu [4]. An order of magnitude analysis of the centrifugal and thermophoretic force though remains to be done to ascertain their individual effects on soot transport.

Figs. 9c & 9d show the pdfs for soot particle diameter. Bigger soot particles are present in case of fuel side vortex since, lower temperatures and lower availability of oxygen close to soot particles allow agglomeration but inhibits oxidation. Again the effect of temperature is dominant due to exponential dependence of the soot production rates on temperature.

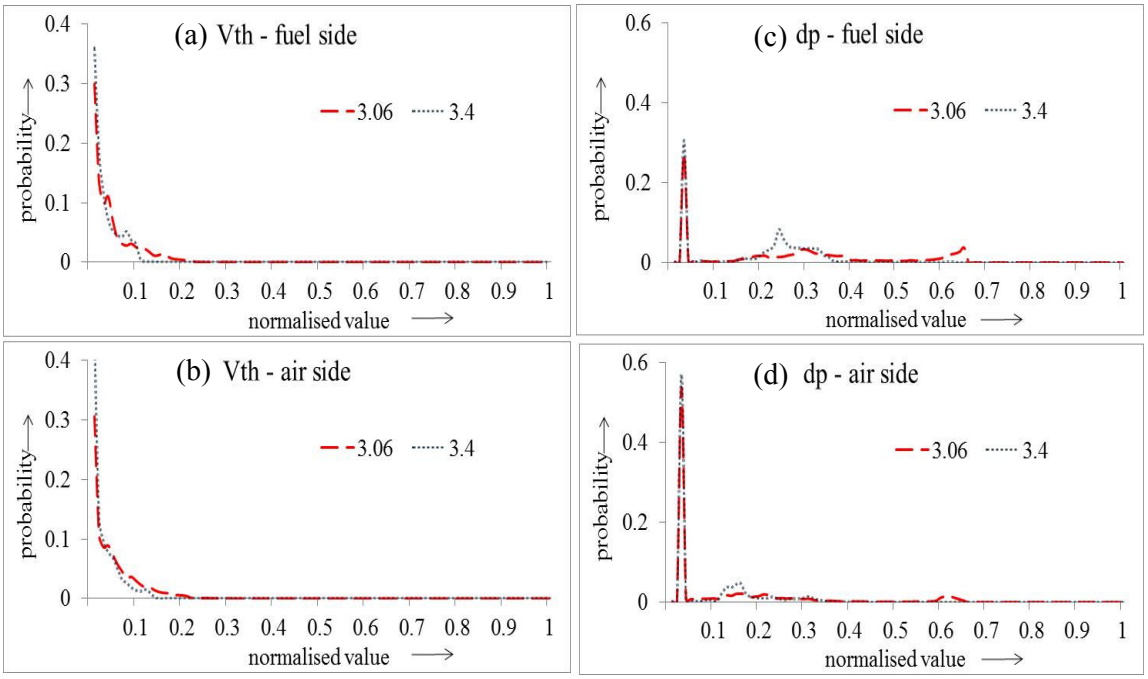

Figure 9. PDFs of thermophoretic velocity and soot diameter: fuel side & air side vortices

CORRELATION COEFFICIENTS

Pearson's correlation coefficient is employed to get a sense of the implications of various parameters on soot mass fraction. For two variables (both data sets) X and Y it is defined as,

$$\rho_{X,Y} = \frac{\mathrm{cov}(X, Y)}{\sigma X \, \sigma Y} \qquad (13)$$

cov(X,Y) is the covariance in X and Y and σX and σY are standard deviations in X and Y respectively. The correlation coefficient of Y_s with other parameters was determined in the domain of statistical study. The results are presented in Figure 10. Y_s has a higher correlation with $[C_2H_2]$ in case of air side vortex (compared to the fuel side vortex) since acetylene present in the vortex core is able to get converted to soot due to higher temperatures. Y_s has a higher correlation coefficient with temperature and acetylene concentration in case of vortex from air side in comparison to the case when vortex is induced from fuel side, which signifies that temperature and acetylene concentration both have important bearings on soot production but the effect of temperature dominates. Effect of transport processes on the soot distribution is more in case of vortex from air side and it helps to distribute the soot in and around the core. This is reflected by a higher (more negative) correlation of Y_s with V_{th} in case of air side vortex. Soot contours are more discrete in case of fuel side vortex since transport processes are not dominant enough so as to bring into effect a more uniform and homogeneous distribution. Air is able to reach the core of the vortex and is able to oxidise the soot in case of air side vortex, which is signified by a more negative and persistent correlation of Y_s with $[O_2]$. Oxidation rates too being exponentially dependent on temperature are higher in case of air side vortex. The soot diameter d_p has decreasing correlation coefficient in case of air side

vortex to signify that smaller soot particles are present in case of air side vortex due more oxidation. In case of fuel side vortex lesser amount of oxidation takes place and hence we have a growing correlation coefficient. This leads to bigger in size but smaller number of soot particles in case of fuel side vortex and smaller in size but more in number and spatially diffuse soot particles in case of air side vortex.

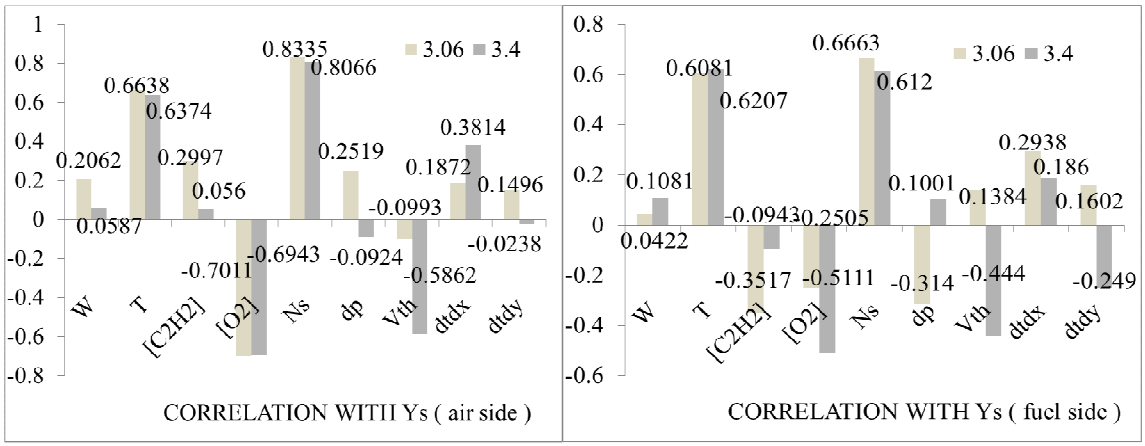

Figure 10. Correlation coefficients with respect to Y_S (air & fuel side vortices)

CONCLUSION

A computational study of the experimental study done in [4] has been presented. The authors incorporated Lindstedt [5] soot model and Lee's soot oxidation [8] model to study the soot formation on flame vortex interaction in a domain and set up same as in [4]. More soot was formed when vortex was introduced from the air side whereas less soot was formed when vortex was introduced from the fuel side, which agrees with [4]. More fuel is present in the fuel stream than required and hence in case of fuel side vortex, fuel is able to push air stream and keep it to the periphery of the vortex leading to lower consumption of fuel. This results in lower temperatures and hence lower soot. Soot is also less in the vortex core compared to air side vortex. In case of air side vortex abundant air at the vortex core results in higher temperature. Acetylene being present in the periphery in higher than required amount results into soot. Higher temperature gradients result in this case. Thus soot is observed in the core in higher amount and in more diffuse layers. This explains to a good extent the reasons behind the observations in [4]. The results were also analysed using statistical tools. Probability density functions and correlation coefficients with respect to Y_s were calculated at two time steps for both air and fuel side vortex. Statistical analysis corroborated our assertion that higher temperature yields more soot in case of air side vortex.

The authors are executing the computational model for smaller time steps and with finer girds to enable bringing more details of the physics behind the observations to the fore, to ensure grid independence and get hold of the finer picture. Various other factors like effects of - strain rate, changes in mass and number density of soot per unit volume due to thermophoretic velocity etc., resulting into the observations are being studied. Studies on conditional probabilities of various parameters are being conducted. The effect of flame stretch and lensing effect are being investigated. Different vortex Reynolds numbers are being applied on the flame to further understand the effects on flame front, its temporal and spatial evolution and on soot production and distribution.

NOMENCLATURE

S total surface area of soot particles
t* non – dimensional time
d_p diameter of soot particles
N_s particle number density of soot
Y_s mass fraction of soot
W vorticity
$\rho_{C(s)}$ density of soot (taken as 2000.0 kg.m3 [5])
ρ density of fluid
e 2.71828
T temperature
s indicates solid state
C_a agglomeration rate (taken as 9.0 [5])
κ Boltzmann's constant
$[C_2H_2]$ molar concentration of acetylene
$[O_2]$ molar concentration of oxygen
α_m accommodating factor
V_{th} Thermophoretic velocity
σX standard deviation in X
σY standard deviation in Y
ν kinematic viscosity
∇T spatial gradient of temperature

REFERENCES

[1] David O. Lignell, Jacqueline H. Chen et.al.; Combustion and Flame 151 (2007) 2–28
[2] Mandal et.al.; Proceedings of the World Congress on Engineering 2007 Vol II WCE 2007, July 2 - 4, 2007, London, U.K.
[3] Pitsch, H., Peters et al. N.(2000) Combustion Science and Technology, 158: 1, 389 — 406
[4] B.M. Cetegen, S. Basu; Combustion and Flame 146 (2006) 687–697
[5] K.M. Leung, R.P. Lindstedt, W.P. Jones ;Combustion and Flame 87 (1991) 289–305
[6] Smooke et al; Combustion and flame, 117:117–139 (1999)
[7] Law et al; Combustion and Flame 151 (2007) 2–28
[8] Lee et al.; Combustion and Flame, vol. 6, 1962, pp. 137 - 145
[9] Kennedy; Models of soot formation and oxidation; Prog. Energy Combust. Sci. Vol. 23, pp. 95-132, 1997
[10] Smooke et al.; Combustion and Flame 143 (2005) 613–628
[11] Lignell et al.; Combustion and Flame 155 (2008) 316–333
[12] Waldmann, L., Z. Naturforschung 14a:589–599(1959)
[13] Waldmann, L., ''On the Motion of Spherical Particles in Nonhomogeneous Gases,'' in Rarefied Gas Dynamics (L. Talbot, ed.), Academic Press, New York, 1961, p. 324.
[14] Suzuki et al., International Journal of Heat and Mass Transfer 52 (2009) 4695–4700
[15] Sagot, Buron et al.; Journal of Aerosol Science 40 (2009) 1030–1049
[16] Pandey et.al. ;Combustion and Flame 148 (2007) 249–262
[17] Xu, Faeth; Combustion and flame 125:804–819 (2001)
[18] Santos, Ferrari et al.; International Communications in Heat and Mass Transfer 36 (2009) 445–450
[19] S.K. Friedlander, Smoke Dust and Haze: Fundamentals of Aerosol Behavior, first ed., Wiley, New York, 197